Journal of Power Sources 196 (2011) 4491–4498

Contents lists available at ScienceDirect

Journal of Power Sources

journal homepage: www.elsevier.com/locate/jpowsour

Palladium-coated manganese dioxide catalysts for oxygen reduction reaction in alkaline media

Wei Sun [a], Andrew Hsu [b], Rongrong Chen [a,*]

[a] Richard G. Lugar Center for Renewable Energy, Indiana University - Purdue University Indianapolis, Indianapolis, IN 46202, USA
[b] Department of Mechanical and Materials Engineering, Wright State University, Dayton, OH 45435, USA

ARTICLE INFO

Article history:
Received 21 November 2010
Received in revised form
24 December 2010
Accepted 7 January 2011
Available online 19 January 2011

Keywords:
Palladium
Manganese dioxide
Oxygen reduction reaction
Alkaline fuel cells
Cathode catalyst

ABSTRACT

Pd-coated manganese dioxide catalysts (Pd@MnO_2) were synthesized by depositing Pd on the surface of β-MnO_2 nanorod particles in aqueous solutions at room temperature. TEM, XRD and electrochemical characterizations indicated that the MnO_2 nanorods were successfully coated with Pd particles when the Pd weight percentage was more than 4.6%. The activities of the Pd@MnO_2 catalysts for oxygen reduction reaction (ORR) were investigated using a rotating disk electrode (RDE) and a rotating ring-disk electrode (RRDE). The ORR onset potentials on the Pd@MnO_2 catalyst shifted positively for more than 250 mV compared with the MnO_2 catalyst without Pd coatings. Both the ORR onset potentials and the limiting current density obtained by the RDE measurements on the Pd@MnO_2 catalysts were close to those on the Pd black catalyst. The mass activity of the Pd@MnO_2 catalysts (normalized by Pd mass) was 2.5 times higher than that of the Pd black catalyst. Based on the Tafel slopes of the Pd@MnO_2 catalysts (which is about 60 mV dec^{-1} at low overpotentials), and based on the fact that the activation energies of the Pd@MnO_2 catalysts are very close to the activation energies of the Pd catalysts, one may conclude that the small amount of Pd coating provides the primary ORR activity of the Pd@MnO_2 catalysts.

1. Introduction

Nanostructured palladium particles, because of their high activities toward oxygen reduction reactions (ORRs), have attracted much attention in recent years as cathode catalysts for fuel cell applications [1–3]. In an alkaline media, Pd nanoparticle catalysts have shown similar ORR activities as Pt nanoparticle catalysts [4,5] and are considered promising replacements for Pt in both traditional alkaline fuel cells and the recently developed solid alkaline fuel cells [6–10]. However, due to Pd's relatively low reserve on earth, it is still too expensive for practical fuel cell applications. Several studies have been conducted in an effort to reduce Pd usage through synthesizing core–shell-like nanoparticles with less expensive metal cores and a Pd shell [11–14].

Manganese dioxide (MnO_2) has been investigated as catalysts and applied in zinc–air batteries and alkaline fuel cells because of its unique electrochemical properties, its low cost, and its environmentally friendly properties [15–19]. MnO_2 is a polymorphic material with a wide variety of structures, e.g., the α, β, or γ forms [20]. The MnO_2 with different structures shows different activities toward the ORR [21]. Among them, β-MnO_2 is composed of a single strand of edge-sharing [MnO_6] octahedron that form a 1X1 tunnel [20]. The thermal stability of β-MnO_2 is much better than α-MnO_2 [22]. In addition, β-MnO_2 with large crystals can be easily produced in large quantities. Recently, one-dimensional β-MnO_2 nanoparticles (nanowires or nanorods) have been synthesized using a hydrothermal method [23–26]. β-MnO_2 with its unique nanostructure is considered one of the promising materials for many catalytic applications [27,28].

The strong interaction between MnO_2 and Pd has been shown to increase the catalytic activity of carbon monoxide (CO) oxidation [29,30]. It has also been shown that the mixture of Pd and MnO_2 has high activity in the air electrode of lithium/air batteries [31,32]. As for the ORR, the synergetic effect between MnO_2 and noble metals was reported by El-Deab et al. [33] and Ding [34]. When MnO_2 was coated on the surface of a Pt electrode, a significant positive shift of the onset potential of the ORR was observed, as compared to that on the bare Pt electrode [33]. In this work, we synthesized core–shell structured, Pd-coated β-MnO_2 nanorod catalysts by using an electroless deposition method. The ORR activities of the Pd@MnO_2 catalysts, as compared with the MnO_2 and Pd black catalysts, were investigated using a rotating disk electrode (RDE) and a rotating ring-disk electrode (RRDE). The performance of the Pd@MnO_2 catalysts in solid alkaline fuel cells was also studied.

* Corresponding author. Tel.: +1 317 274 4280; fax: +1 317 274 0789.
E-mail address: rochen@iupui.edu (R. Chen).

0378-7753/$ – see front matter © 2011 Elsevier B.V. All rights reserved.
doi:10.1016/j.jpowsour.2011.01.031

2. Experimental

2.1. Catalyst synthesis

Manganese dioxide (β-MnO_2) was synthesized using a hydrothermal method as reported in Refs. [35,36]. $KMnO_4$ and $MnSO_4$ (Fisher Scientific, USP grade) were used to prepare aqueous solutions with concentrations of 0.1 and 0.6 M, respectively. 30 ml of the prepared $KMnO_4$ aqueous solution was added to 30 ml of the $MnSO_4$ solution drop by drop at room temperature while stirring vigorously in a beaker. Then, the mixture was transferred into a Teflon-lined autoclave reactor (100 ml, Parr Instrument Co.). The autoclave was sealed and heated to 140 °C at a rate of 4 °C min^{-1} and maintained at this temperature for 12 h while continuously stirring. After completing the reaction, the autoclave reactor was cooled down to room temperature. The suspension thus obtained was filtered using a Buchner filter funnel. The filtered solid was washed with ultrahigh pure DI water (resistivity of 18 MΩ cm^{-1}). Then, the solid was dried overnight in an oven at 80 °C. The ascertainment of the product as β-MnO_2 using XRD is reported in Section 3.

Pd-coated manganese dioxide (Pd@MnO_2) was synthesized by chemically reducing the palladium precursor onto the MnO_2 particles as follows: (1) 0.25 g of $SnCl_2$ (MP Biomedicals) was dissolved into 50 ml DI water; 0.2 g of the prepared MnO_2 was added to the solution; the mixture was stirred for 30 min for sensitization pretreatment; the sensitized MnO_2 was separated and washed with DI water and redistributed into 40 ml of water to form a suspension. (2) $PdCl_2$ (MP Biomedicals) was prepared as an aqueous solution with a concentration of 0.0225 M. An amount of 1 ml of the $PdCl_2$ solution was added to the MnO_2 suspension drop by drop while stirring constantly. (3) 40 ml of a 0.05 M citric acid solution (MP Biomedicals) was added to the $PdCl_2$/MnO_2 aqueous solution. (4) The pH value of the suspension was adjusted to about 8 by adding 1 M of a KOH (Acros, ACS grade) solution. (5) 10 ml of $NaBH_4$ (Strem Chemicals) with a concentration of 0.1 M was added to the suspension drop by drop. (6) After 30 min, the solid precipitate was filtered, using a Buchner filter funnel, and washed with DI water until the pH of the filtrate became 7. (7) The prepared sample was dried overnight in an oven at 80 °C with a negative pressure of 25 PSI.

In the procedures described above, the amount of the $PdCl_2$ solution that was added to the MnO_2 suspension during step (2) was used to determine the molar ratio of Pd to Mn in the catalyst. For example, when 1 ml of the $PdCl_2$ solution with a concentration of 0.0225 M was added to the MnO_2 suspension, the catalyst obtained had a molar ratio of Pd to Mn of 1:99; the weight percentage of Pd in the Pd@MnO_2 catalyst was 1.2 wt.% (denoted as: 1.2 wt.%Pd@MnO_2). Similarly, by increasing the volume of $PdCl_2$ added to the MnO_2 suspension, catalysts with a Pd to Mn molar ratio of 2:98, 4:96, and 8:92 were obtained, and the corresponding weight percentages of Pd in the catalysts were 2.3% (2.3 wt.%Pd@MnO_2), 4.6% (4.6 wt.%Pd@MnO_2), and 8.7% (8.7 wt.%Pd@MnO_2), respectively.

2.2. Physical characterization

Morphologies of the prepared catalysts were investigated by using a Tecnai G^2 TWIN/BioTWIN transmission electron microscope (FEI Company) operated at 80 kV. X-ray diffraction (XRD) patterns of the MnO_2 and Pd@MnO_2 catalysts were recorded with a Siemens X-ray diffractometer using Cu Kα radiation with a Ni filter. The tube current was 30 mA with a tube voltage of 40 kV. The 2θ angular regions between 10 and 90° were explored at a scan rate of 4° min^{-1}.

2.3. Electrochemical characterization

A catalyst ink was prepared by dispensing 5 mg of the synthesized catalyst, 5 mg of carbon (Black Pearls 2000, CABOT), and 50 μl of Nafion solution (5 wt.%, Sigma–Aldrich) into 5 ml of ethanol. For the comparison, Palladium black (Strem Chemicals) ink was prepared using the same procedure. After the ink was sonically produced in an ultrasonic bath, 20 μl of the catalyst ink was transferred onto the surface of a glassy carbon rotating ring disk electrode (RRDE) (5.0 mm disk diameter with a platinum ring, Pine Instruments). After evaporating the ethanol via air flow, a thin layer of catalyst was formed on the surface of the disk electrode. The RRDE was mounted to a rotator (AFMSRCE, Pine Instruments) and characterized by either an advanced electrochemical system M2273 (PAR) or a bipotentiostat (AFCBP1, Pine).

The electrochemical experiments were carried out in a three-electrode electrochemical cell with a jacket. The cell temperature was controlled by recycling water between the jacket and a water bath through a water pump (NESLAB). The working electrode was immersed in a 0.1 M KOH solution saturated with either argon or oxygen (Praxair). A gold wire was used as a counter electrode. An Hg/HgO reference electrode was used through a salt bridge, and all the potentials in this work were referred to the Hg/HgO in a 0.1 M KOH solution. The overpotential of the working electrode toward the ORR was determined by the potential applied to the working electrode and the equilibrium potential of the ORR in a 0.1 M KOH solution (E^0 = 0.401 V vs. NHE). The thermodynamic shift of the equilibrium potential of the ORR with temperature was corrected by an equation reported in the literature [37].

Hydrogen peroxide production in the oxygen-saturated 0.1 M KOH solution was monitored using a RRDE with a polycrystalline Pt ring potential biased at 0.1 V vs. Hg/HgO (collection efficiency of the ring electrode $N = I_{ring}/I_{disk} = 0.21$). Hydrogen peroxide yields were calculated with the equation as described in the literature [38].

2.4. Fuel cell performance test

The synthesized Pd@MnO_2 catalysts, together with 15 wt.% carbon (Black Pearls 2000, CABOT), were employed to prepare a cathode for an alkaline fuel cell using anion exchange membranes. Pt/C (50 wt.%) (Johnson & Matthey) was used to prepare an anode. The catalyst slurries were prepared by mixing the catalysts with anion ionomer (20 wt.%) and ethanol in an ultrasonic bath for 1 h. The catalyst slurries were pasted onto the gas diffusion layers (GDL LT 1200-W, Fuel Cell Store) with a catalyst loading of 2.5 mg cm^{-2} in both the cathode and the anode. The membrane electrode assembly (MEA) was formed by directly pressing the prepared anode and cathode onto a piece of polysulfone membrane, which was prepared as described by Wang et al. [39]. The prepared MEA was assembled into a fuel cell and tested by a fuel cell testing system (850e, Scribner Associates, Inc.), while the hydrogen and oxygen (100% humidity) were fed at a flow rate of 0.2 lpm.

3. Results and discussion

3.1. Physical characterization

Fig. 1a shows the XRD patterns of the prepared MnO_2 materials and can be indexed as a pure tetragonal phase [space group: $P42/mnm$ (136)] of β-MnO_2 with lattice constants a = 4.3980 Å and c = 2.8760 Å (PDF#24-0735). Fig. 1b, c shows the XRD patterns of the Pd-coated MnO_2 catalysts with a Pd coating of 1.2 wt.% and 8.7 wt.%, respectively. When the MnO_2 was coated with Pd, small peaks located at about 40.1°, 46.7°, 68.1° were observed. Accord-

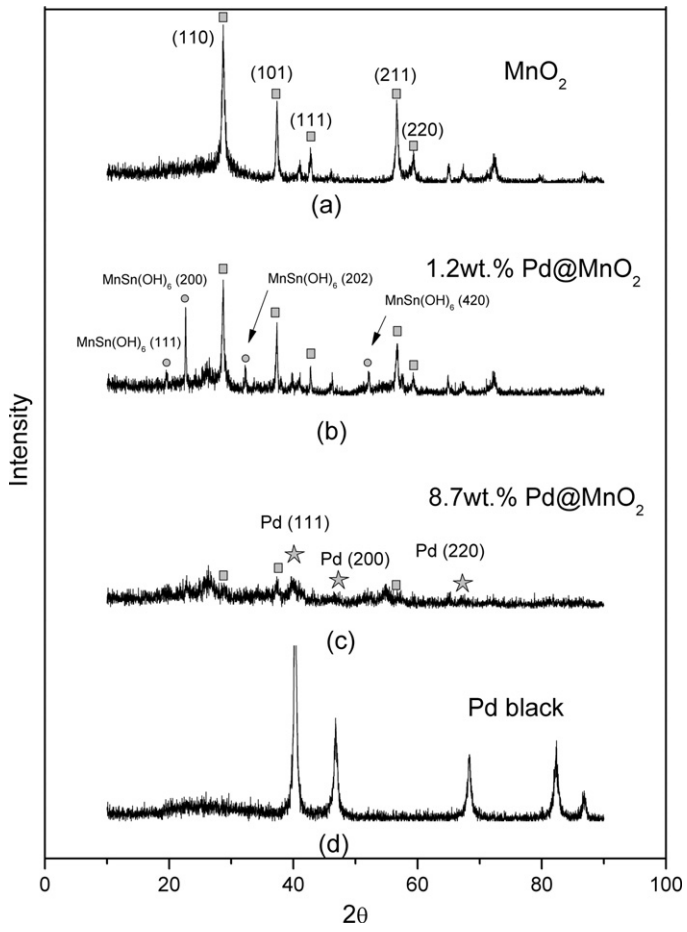

Fig. 1. X-ray diffraction (XRD) patterns for the synthesized Pd@MnO_2 catalysts (b, c). The results for the uncoated-MnO_2 (a) and Pd black (d) are included for comparison.

ing to the powder diffraction file (PDF#65-2867), the peaks were attributed to the Pd(1 1 1), Pd(2 0 0) and Pd(2 2 0), respectively, which were also confirmed by XRD patterns of Pd black catalysts (with average particle size of 17.2 nm). These peaks became much more obvious when the Pd was increased to 8.7 wt.%. For the sample of 1.2 wt.%Pd@MnO_2 (Fig. 1b), some peaks that belonged to $MnSn(OH)_6$ were observed (PDF#25-0553), which indicates that a small amount of $MnSn(OH)_6$ existed in the catalyst. $MnSn(OH)_6$ can form during the MnO_2 sensitization process in an alkaline media. As a reducing reagent, $MnSn(OH)_6$ can reduce Pd^{2+} to Pd on the surfaces of the MnO_2 nanorods. When the amounts of $PdCl_2$ were low, large portions of the MnO_2 surfaces still had $MnSn(OH)_6$ that had not reacted. When the amounts of $PdCl_2$ were increased, the surfaces of the MnO_2 nanorods were covered with Pd, and $MnSn(OH)_6$ was no longer observed (shown in Fig. 1c).

TEM images of the synthesized MnO_2 materials are shown in Fig. 2a, b. Nanorod crystals with diameters of 40–50 nm and lengths of 500–1000 nm can be observed in the images. The surfaces of the MnO_2 crystals were clean and smooth. Fig. 2c–e shows TEM images of Pd-coated MnO_2 catalysts. When the amount of Pd coating was 2.3 wt.% (Fig. 2c), Pd particles were observed on the MnO_2 nanorods. Their average diameter, estimated from the TEM images, was about 10 nm. When the amount of Pd coating increased to 4.6 wt.%, the number of Pd particles increased and the estimated diameter of Pd particles increased to about 25 nm. When the amount of Pd coating increased to 8.7 wt.%, most of the surfaces of the MnO_2 nanorods were covered by the Pd particles and the Pd particles can no longer be easily distinguished individually. From the TEM and XRD results, we can conclude that we have successfully synthesized Pd-coated MnO_2 nanorod catalysts using the methods described in Section 2.

3.2. Cyclic voltammetry

Fig. 3a shows the cyclic voltammetry (CV) curves of the MnO_2 and Pd@MnO_2 catalysts in 0.1 M KOH solutions saturated with argon. For the uncoated β-MnO_2, a featureless CV curve was observed. In the potential range from −0.80 to 0.40 V, the CV curve of the β-MnO_2 revealed a high charging–discharging pseudocapacitive current, which agrees with what was reported by others [40,41]. For the Pd@MnO_2 catalysts, the pseudocapacitive currents were reduced significantly due to the Pd coverage on the MnO_2 surface. However, a clear peak appeared at about −0.24 V during the cathodic scanning. Compared to the CV curves of the Pd black in alkaline media (top of Fig. 3a) and what have been reported [42,43], the peak could be attributed to the reduction of PdO. When the Pd loadings on the MnO_2 increased, the peak current at −0.24 V increased accordingly. The synthesized Pd@MnO_2 catalysts show some characteristics similar to those observed on Pd black catalysts.

In order to further distinguish the difference of the electrocatalytic properties between the MnO_2 and the Pd@MnO_2 catalysts, the catalysts were mixed with carbon material (Black Pearls 2000, 50 wt.%) to improve their electrical conductivity. The CV curves of carbon-mixed MnO_2 and Pd@MnO_2 catalysts (denoted as MnO_2/C and Pd@MnO_2/C, respectively) are shown in Fig. 3b. The CV curve of the carbon-supported uncoated MnO_2 catalyst shows a quasi-reversible characteristic, which agrees with previously reported results [27]. During the cathodic scanning, a significant sluggish reduction peak appeared between 0 and −0.2 V. Small reduction peaks appeared at about −0.2 V and −0.27 V. A small peak was also observed at about −0.7 V. According to previously reported XANES results [28], these peaks may be ascribed to the reduction of Mn(IV) to Mn(III) at about −0.1 V, then through Mn_3O_4 (∼−0.27 V) and converted to Mn(II) at about −0.7 V. During the anodic scanning, an obvious oxidation peak was observed at about 0.05 V, which could be ascribed to the oxidation of Mn(II) to Mn(III). When MnO_2 was coated with Pd nano-particles, the cathodic peaks located at −0.1 V and the anodic peak located at 0.05 V, related to the changes of the Mn valence states, can still be observed though the peaks are greatly weakened. With the increase of Pd loading, the peak that belongs to the reduction of PdO (∼−0.24 V) appeared and became significant, and the Pd oxidation current increased at the potential higher than 0.2 V. In the CV curve of Pd black/C, the peaks located in the range of −0.7 V to −0.6 V can be attributed to the hydrogen adsorption and desorption [44]. Because the amount of Pd loading in the Pd@MnO_2 catalysts was very small, the hydrogen adsorption and desorption peaks in this region became less noticeable for the catalysts with or without carbon. The CV results confirmed that Pd was coated on the surface of the MnO_2, and the coated Pd had different electrochemical characteristics from the pure Pd black catalyst.

3.3. RDE measurements

Fig. 4a shows the ORR anodic polarization curves obtained on the Pd@MnO_2 catalysts without carbon. As a comparison, the results of pure β-MnO_2 are also shown in this figure. From the ORR polarization curves, we can see that the activity of the pure β-MnO_2 toward the ORR is much lower compared to the Pd@MnO_2 catalysts. When the β-MnO_2 was coated with Pd (4.6 or higher wt.%), the ORR onset potential and half-wave potentials ($E_{1/2}$) on the Pd@MnO_2 catalysts shifted positively by more than 250 mV, which can be due to that most of the surface of the MnO_2 was covered by Pd nano-particles.

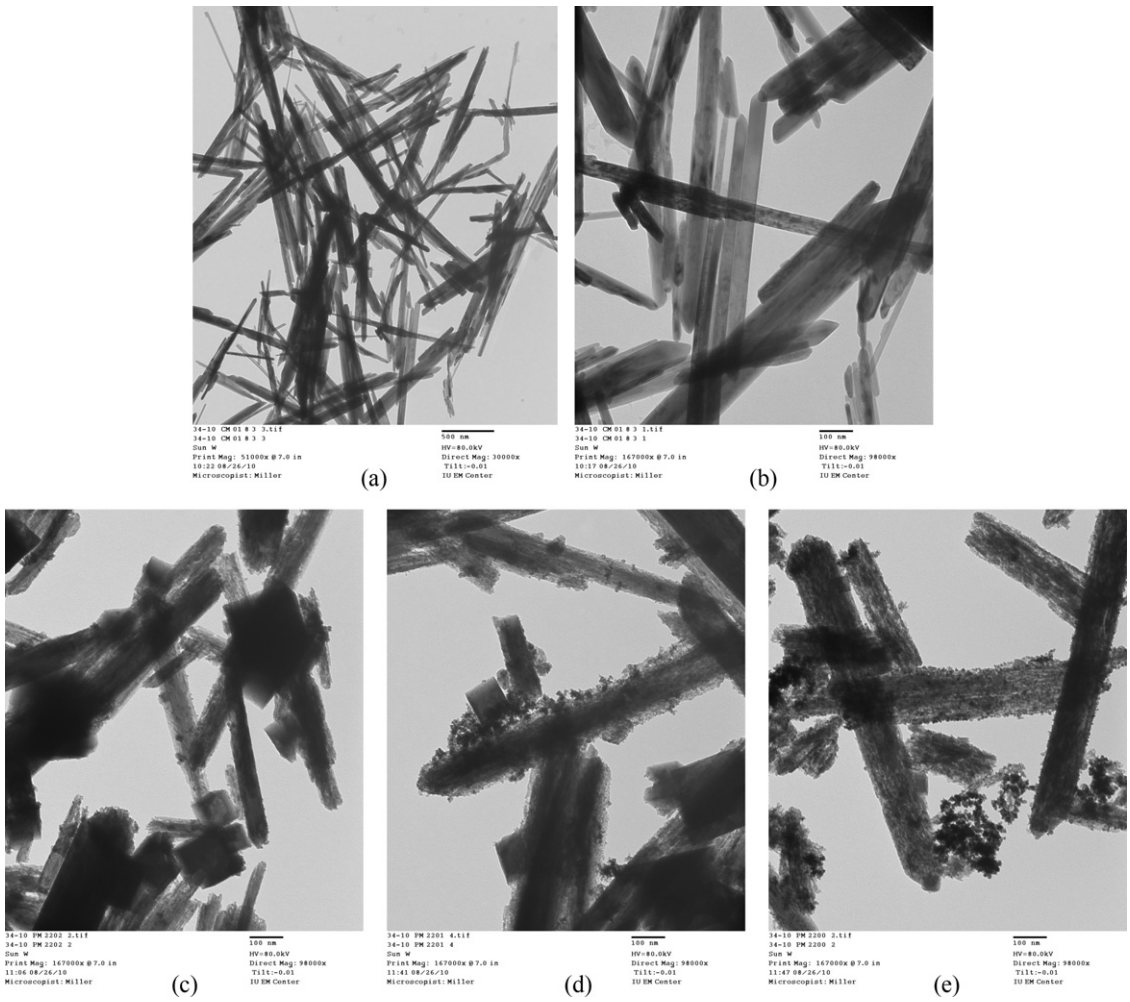

Fig. 2. TEM images of synthesized MnO_2 (a, b) and Pd@MnO_2 catalysts with Pd 2.3 wt.% (c); 4.6 wt.% (d) and 8.7 wt.% (e).

(Fig. 2d) and the ORR mainly occurred on the surface of the Pd. In addition, the coating of Pd may have increased the electronic conductivity of the nanosized MnO_2 particles, which is similar to what observed with silver on the MnO_2 [45]. However, the ORR onset (and $E_{1/2}$) potentials and the limiting currents on the Pd@MnO_2 catalysts are still not as high as that on the Pd black catalysts.

Fig. 4b shows the ORR polarization curves obtained on the Pd@MnO_2 catalysts mixed with carbon. By comparing Fig. 4a and b, we can see the effect of carbon on the activity of the various catalysts: from the polarization curve of the Pd black with and without carbon, it appears that the effect of carbon was not significant. However, the effect of carbon on the activity of β-MnO_2 is quite obvious. The onset potential shifted positively about 150 mV; the current density at −0.6 V increased 4 times and reached the limiting state. This can be explained by the synergetic effect between carbon and MnO_2 [16]. As for the Pd@MnO_2 catalyst, the effect of carbon on the onset potential and limiting current density was in-between of those on Pd and MnO_2. For example, the current density of the 4.6 wt.%Pd@MnO_2/C catalyst increased 2 times and reached a limiting state of 6.8 mA cm^{-2}, the same as the limiting current density of Pd black/C catalyst. All the carbon supported MnO_2 and Pd@MnO_2 catalysts show more positive ORR onset and $E_{1/2}$ potentials, and higher limiting currents than that on the carbon support alone, which indicated that the MnO_2 played a beneficial role for promoting the ORR in alkaline media. When the Pd coating on the MnO_2 was low (<4.6 wt.%), the beneficial effect of the MnO_2 on the ORR was more significant because the surface of the MnO_2 was not completely covered by the Pd particles as observed in the TEM images and the CV results. With the increasing of the Pd coatings, the role that Pd played became more significant. But the beneficial role of MnO_2 cannot be ignored.

Fig. 5 shows the kinetic current density and mass activity of various catalysts normalized by the Pd mass. For proton exchange membrane (PEM) fuel cells, the kinetic current of the catalysts at 0.9 V (vs. RHE) is usually used to calculate the mass activity [46]. Here we obtained the kinetic current density at −0.090 V (vs. Hg/HgO), which corresponded to the same overpotential as 0.9 V in a PEM fuel cell. From Fig. 5, we can see that the kinetic current density of Pd black/C, 17.8 mA cm^{-2}, is much higher than all the prepared Pd@MnO_2/C catalysts. However, the mass activities of Pd@MnO_2/C catalysts were significantly higher than that on Pd black/C catalysts. With the increasing Pd coatings, the mass activity of the Pd@MnO_2/C catalysts also increased. When the Pd was coated with 8.7 wt.%, the mass activity became 2.5 times higher than that of Pd black under the same experimental conditions, which can be attributed to the high surface of nano-Pd particles on MnO_2 and the beneficial effect of MnO_2. The carbon-supported palladium (Pd/C) for the ORR has been reported [1,38]. A comparison of the mass activity of the Pd/C and Pd@MnO_2 catalysts, the 8.7 wt.% Pd@MnO_2 catalyst shows similar mass activity as the Pd/C (0.5 mA μg^{-1}) with particle size ∼17 nm, and less than the Pd/C with small nano-particle size (3 nm) [1]. After optimizing the morphology of Pd coating on the MnO_2, the ORR activities of the Pd@MnO_2/C catalyst will be further improved.

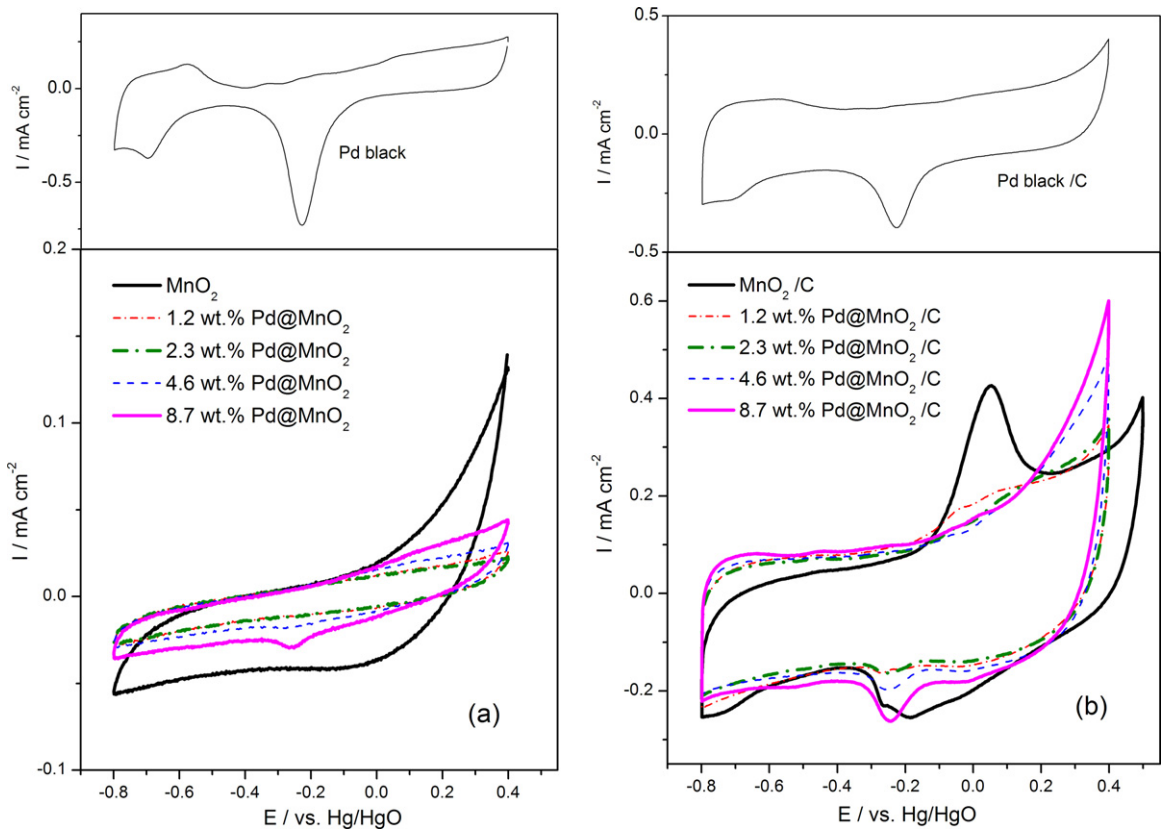

Fig. 3. Cyclic voltammograms of the Pd@MnO_2 catalysts (a) and Pd@MnO_2/C catalysts (b) in a 0.1 mol L^{-1} KOH solution saturated with argon at room temperature. The scan rate was 10 mV s^{-1}. The rotating speed was 1600 rpm.

3.4. ORR selectivity on Pd-coated MnO_2 catalysts

The selectivity of the catalyst toward the ORR was studied using RRDE measurements. The RRDE test results are shown in Fig. 6. The obtained H_2O_2 yields are shown in Table 1. As a benchmark, the H_2O_2 yield on the Pd black/C was measured; the yield was as low as 1.4%, which is in agreement with the Pd/C and Pt/C catalysts at room temperature [38,47]. The H_2O_2 yield on the β-MnO_2/C catalyst was obtained at about 5.4%. For the 1.2 wt.%Pd@MnO_2/C catalyst, a reduction in the H_2O_2 yield (~4.6%) was observed. With the increase of Pd coating to either 2.3 wt.% or 4.6 wt.%, the H_2O_2 yield further decreased to 3.6% and 2.9%, respectively. When the coating of Pd increased to 8.7 wt.%, the H_2O_2 yield decreased to 1.9%, which was very close to that observed on the Pd black/C, 1.4%. The RRDE results indicated that the surfaces of the MnO_2 particles were mostly covered by the Pd coating when the Pd coating was

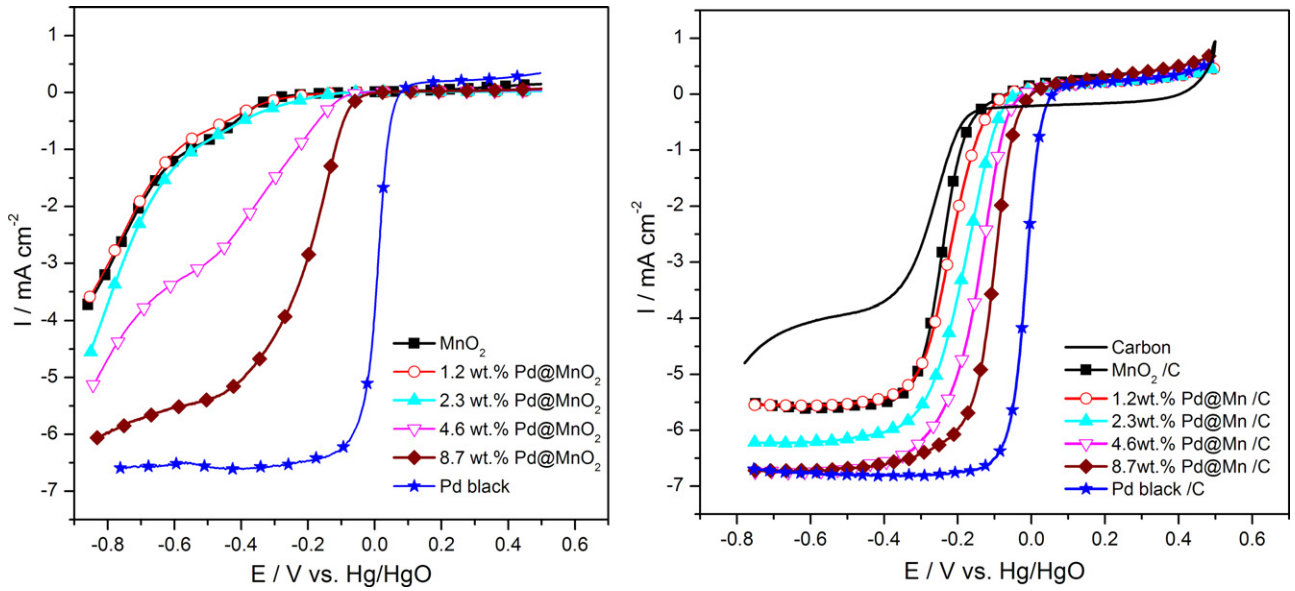

Fig. 4. Polarization curves of the Pd@MnO_2 catalysts (a) and Pd@MnO_2/C catalysts (b) in a 0.1 mol L^{-1} KOH solution saturated with oxygen at room temperature. The scan rate was 10 mV s^{-1}. The rotating speed was 2500 rpm.

Table 1
The HO_2^- fractional yields obtained from RRDE experiments.

	MnO_2	1.2 wt.% Pd@MnO_2/C	2.3 wt.% Pd@MnO_2/C	4.6 wt.% Pd@MnO_2/C	8.7 wt.% Pd@MnO_2/C	Pd black/C
HO_2^- fractional yields	5.4%	4.6%	3.6%	2.9%	1.9%	1.4%

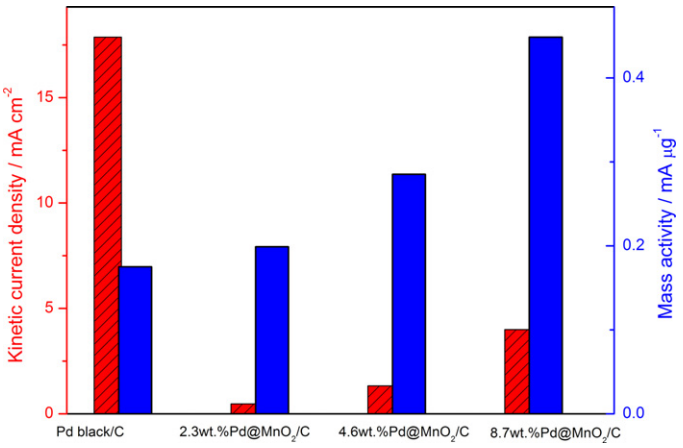

Fig. 5. Kinetic current density of the Pd@MnO_2/C catalysts obtained at −0.09 V (vs. Hg/HgO, 0.1 M KOH) from Fig. 4b and corresponding mass activity in terms of Pd mass.

higher than 4.6 wt.% and showed similar ORR characteristics to that of Pd/C.

3.5. Activation energy of the catalyst toward ORR

Fig. 7a, b shows the Tafel plots of the ORR on the Pd@MnO_2/C catalysts with Pd coating at 4.6 wt.% and 8.7 wt.% at various temperatures. The Tafel plots were derived from the ORR polarization curves at the corresponding temperatures with a rotation rate at 2500 rpm. The Tafel plots can be divided into two regions: (1) when the potential is higher than −0.15 V (vs. Hg/HgO), the Tafel slope is about 56 mV dec^{-1} for 4.6 wt.% Pd@MnO_2/C and 61 mV dec^{-1} for 8.7 wt.% Pd@MnO_2/C; (2) when the potential is lower than −0.15 V (vs. Hg/HgO), the Tafel slope is about 128 mV dec^{-1} for 4.6 wt.% Pd@MnO_2/C and 132 mV dec^{-1} for 8.7 wt.% Pd@MnO_2/C. The Tafel slope at a low overpotential was maintained at about 60 mV dec^{-1}, which is in agreement with that of Pd black (shown in Fig. 7a) and Pd/C [38]. This suggests that the catalytic mechanism for the ORR on the Pd@MnO_2/C catalyst is likely to be similar to that of the Pd catalyst [48,49]. On both the 4.6 wt.%Pd@MnO_2/C and the 8.7 wt.% Pd@MnO_2/C catalysts, the kinetic currents, i_k, increased continuously with the increase of temperature. It was also observed that the kinetic current of the 8.7 wt.%Pd@MnO_2/C catalyst was slightly higher than that of the 4.6 wt.% Pd@MnO_2/C catalyst at a fixed potential. Fig. 7c shows the Arrhenius plots of the ORR on both the 4.6 wt.% Pd@MnO_2/C and the 8.7 wt.% Pd@MnO_2/C catalysts. The ORR apparent activation energies were calculated from the Arrhenius plots, and the result are shown in Table 2. The activation energy of the ORR on the 4.6 wt.% Pd@MnO_2/C decreased from 30.7 kJ mol^{-1} to 22.2 kJ mol^{-1} when the overpotential increased from 0.30 V to 0.40 V. At the same overpotential, the activation energy of the 8.7 wt.% Pd@MnO_2/C was lower than that of the 4.6 wt.% Pd@MnO_2/C. Jiang et al. reported that the activation energy of Pd/C was 30–40 kJ mol^{-1} when the overpotential was in the range of 0.3–0.4 V [38]. Our results show that the activation energy of Pd@MnO_2/C is in the same range as that of Pd/C and Pt/C catalysts [38].

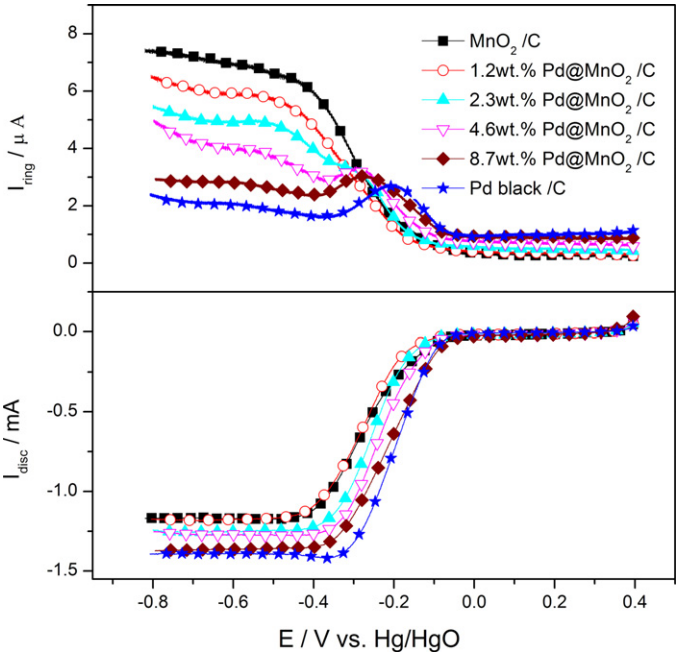

Fig. 6. The RRDE experimental results of the Pd@MnO_2/C catalysts. KOH solution: 0.1 mol L^{-1}, saturated with oxygen; scan rate: 10 mV s^{-1}; rotating speed: 2500 rpm. The potential of the ring electrode was set to 0.1 V (vs. Hg/HgO).

3.6. Fuel cell performance test

Fig. 8 shows the galvanostatic current (i)–voltage (E) curves and power curves of performance of anion exchange membrane fuel cells (AEMFCs) that were assembled using different cathodes (built with 4.6 wt.%Pd@MnO_2/C and β-MnO_2/C catalysts, respectively) but identical anodes and membranes. The i–E curves were recorded point-by-point with increasing current. The performance of the AEMFCs was dependent on the cathode catalyst used. The results show that the OCV of the fuel cell using Pd@MnO_2/C was 1.02 V, about 120 mV higher than that of the β-MnO_2/C. The fuel cell using Pd@MnO_2/C showed a much higher performance compared with that using the β-MnO_2/C. The maximum power density, 66 mW cm^{-2}, was almost 2 times that of the β-MnO_2 without Pd coating. The linear region of the i–E curves shows that the ohmic polarization of the MEA using the Pd@MnO_2/C catalyst is much lower than that of the β-MnO_2/C MEAs, which indicated a better electronic conductivity on the Pd@MnO_2 cathode than the β-MnO_2/C cathode. The fuel cell performance test results demonstrated that the Pd@MnO_2 catalysts can be successfully used in the cathode of the AEMFC. Further work is currently being carried out to improve Pd utilization and the performances of the Pd@MnO_2 catalysts and the fuel cell.

Table 2
The calculated activation energy of the Pd@MnO_2/C catalysts at different overpotentials.

	Overpotential, V		
	0.30	0.35	0.40
4.6 wt.% Pd@MnO_2/C, kJ mol^{-1}	30.7	28.5	22.2
8.7 wt.% Pd@MnO_2/C, kJ mol^{-1}	28.8	27.3	21.7

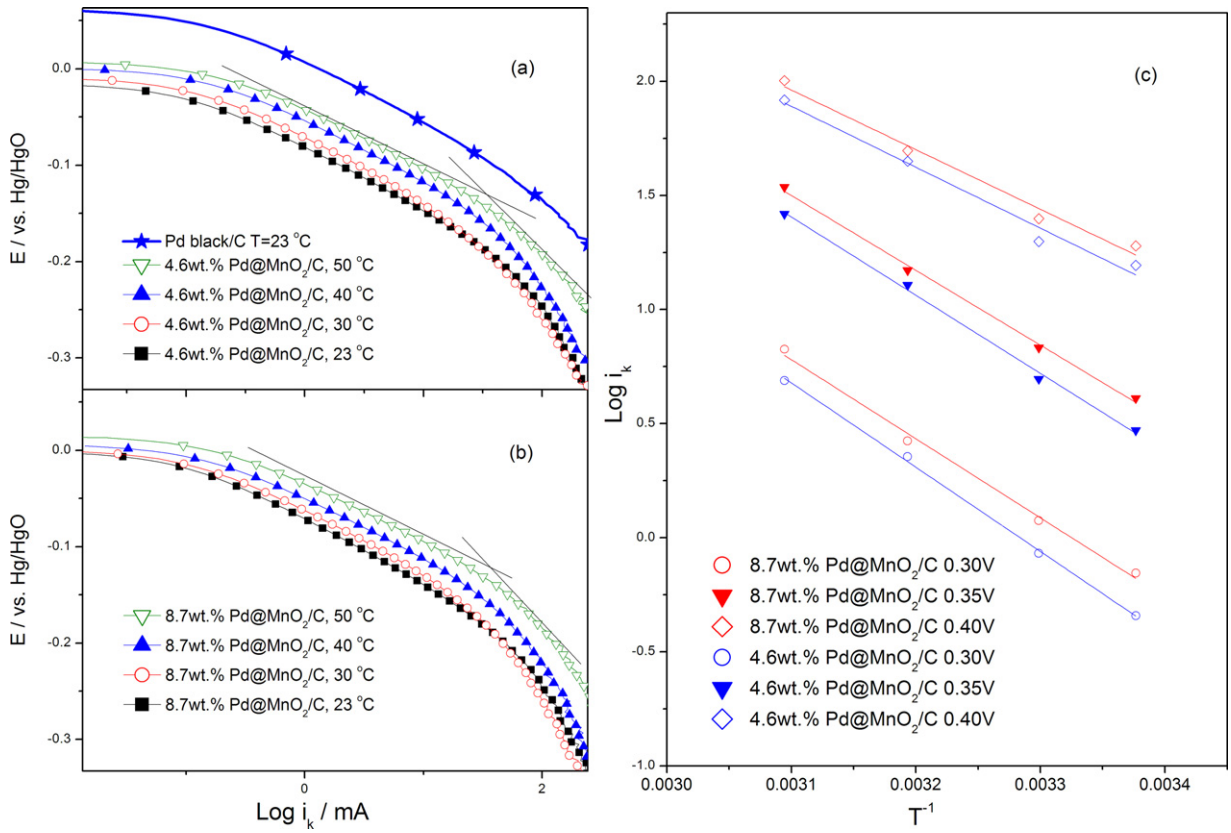

Fig. 7. Tafel plots of the ORR on 4.6 wt.%Pd@MnO_2/C catalyst (a) and 8.7 wt.%Pd@MnO_2/C catalyst (b) at different temperatures with a rotation rate of 2500 rpm and the corresponding Arrhenius plots at overpotentials of 0.30, 0.35, and 0.40 V between 23 °C and 50 °C (c). The electrolyte of 0.1 M KOH was saturated with O_2. The scan rate was 10 mV s^{-1}.

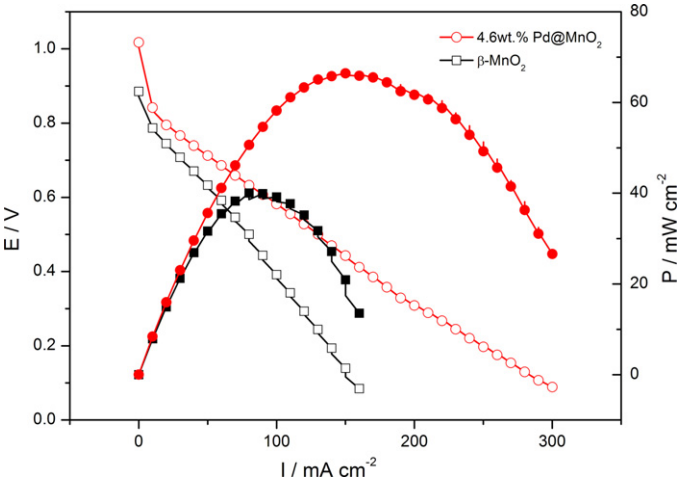

Fig. 8. Performance of the alkaline fuel cell using 4.6 wt.% Pd@MnO_2/C catalyst and uncoated β-MnO_2 in the cathode. The temperature was 60 °C, and the backpressure was 10 PSI.

4. Conclusion

A Pd-coated β-MnO_2 nanorod catalyst was synthesized. TEM, XRD, and electrochemical characterization confirmed that Pd dominated the surfaces of the β-MnO_2 particles when they were coated with more than 4.6 wt.%. The Pd-coated catalyst showed higher activity toward ORR than the uncoated MnO_2 catalyst: when the Pd coating was higher than 4.6 wt.%, the onset potential and half wave potential of the Pd@MnO_2 catalyst shifted positively by more than 250 mV compared to that of the pure MnO_2 catalyst to a value that is close to that of Pd black. For the same 4.6 wt.% Pd@MnO_2 catalyst, the limiting current density reached 6.8 mA cm^{-2}, which is comparable to that of Pd black. The mass activity (based on Pd) of the synthesized catalyst increased to 2.5 times that of the Pd black catalyst. The higher activity of the synthesized catalyst was attributed to the Pd coating on the surface of the nanorod MnO_2 and the beneficial role of MnO_2. The coated Pd played an important role in the ORR, which was confirmed by Tafel slopes with a 60 mV dec^{-1} at low overpotential, and the activation energies were very close to that of the pure Pd catalysts. The low cost and high performance Pd@MnO_2 catalysts are promising as cathodic catalysts in alkaline fuel cells.

Acknowledgment

This work was supported by the U.S. Army Research Lab (Grant No. W911NF-07-2-0036).

References

[1] L. Jiang, A. Hsu, D. Chu, R. Chen, J. Electrochem. Soc. 156 (2009) B643–B649.
[2] Y. Lin, X. Cui, X. Ye, Electrochem. Commun. 7 (2005) 267–274.
[3] J. Moreira, P. del Angel, A.L. Ocampo, P.J. Sebastián, J.A. Montoya, R.H. Castellanos, Int. J. Hydrogen Energy 29 (2004) 915–920.
[4] F.H.B. Lima, J. Zhang, M.H. Shao, K. Sasaki, M.B. Vukmirovic, E.A. Ticianelli, R.R. Adzic, J. Phys. Chem. C 111 (2007) 404–410.
[5] L. Xiao, L. Zhuang, Y. Liu, J.T. Lu, H.D. Abruna, J. Am. Chem. Soc. 131 (2009) 602–608.
[6] J.R. Varcoe, R.C.T. Slade, E. Lam How Yee, Chem. Commun. (2006) 1428–1429.
[7] Y.W. Guigui Wang, D. Chu, R. Chen, D. Xie, J. Membr. Sci. (2009).
[8] L. Li, Y.X. Wang, J. Membr. Sci. 262 (2005) 1–4.
[9] J. Zhou, M. Unlu, J.A. Vega, P.A. Kohl, J. Power Sources 190 (2009) 285–292.
[10] S. Gu, R. Cai, T. Luo, Z. Chen, M. Sun, Y. Liu, G. He, Y. Yan, Angew. Chem. 121 (2009) 6481.
[11] L.D. Pachon, M.B. Thathagar, F. Hartl, G. Rothenberg, PCCP 8 (2006) 151–157.

[12] M.N. Nadagouda, R.S. Varma, Cryst. Growth Des. 7 (2007) 2582–2587.
[13] G.J. Zhou, M.K. Lu, Z.S. Yang, Langmuir 22 (2006) 5900–5903.
[14] E. Callini, L. Pasquini, E. Piscopiello, A. Montone, M.V. Antisari, E. Bonetti, Appl. Phys. Lett. 94 (2009).
[15] I. Roche, E. Chainet, M. Chatenet, J. Vondrak, J. Phys. Chem. C 111 (2006) 1434–1443.
[16] M.L. Calegaro, F.H.B. Lima, E.A. Ticianelli, J. Power Sources 158 (2006) 735–739.
[17] Y.L. Cao, H.X. Yang, X.P. Ai, L.F. Xiao, J. Electroanal. Chem. 557 (2003) 127–134.
[18] M. Lanqun, T. Sotomura, K. Nakatsu, N. Koshiba, Z. Dun, T. Ohsaka, J. Electrochem. Soc. 149 (2002) A504–A507.
[19] F.H.B. Lima, M.L. Calegaro, E.A. Ticianelli, J. Electroanal. Chem. 590 (2006) 152–160.
[20] S. Devaraj, N. Munichandraiah, J. Phys. Chem. C 112 (2008) 4406–4417.
[21] F. Cheng, Y. Su, J. Liang, Z. Tao, J. Chen, Chem. Mater. 22 (2009) 898–905.
[22] X. Zhang, W.S. Yang, J.J. Yang, D.G. Evans, J. Cryst. Growth 310 (2008) 716–722.
[23] I.Y. Kim, H.W. Ha, T.W. Kim, Y. Paik, J.H. Choy, S.J. Hwang, J. Phys. Chem. C 113 (2009) 21274–21282.
[24] N. Wang, H.T. Pang, H.R. Peng, G.C. Li, X.G. Chen, Cryst. Res. Technol. 44 (2009) 1230–1234.
[25] Y. Jia, J. Xu, L. Zhou, H. Liu, Y. Hu, Mater. Lett. 62 (2008) 1336–1338.
[26] Y.G. Zhang, L.Y. Chen, Z. Zheng, F.L. Yang, Solid State Sci. 11 (2009) 1265–1269.
[27] S. Jana, S. Basu, S. Pande, S.K. Ghosh, T. Pal, J. Phys. Chem. C 111 (2007) 16272–16277.
[28] F.H.B. Lima, M.L. Calegaro, E.A. Ticianelli, Electrochim. Acta 52 (2007) 3732–3738.
[29] A.V. Salker, R.K. Kunkalekar, Catal. Commun. 10 (2009) 1776–1780.
[30] J.S. Park, D.S. Doh, K.Y. Lee, Top. Catal. 10 (2000) 127–131.
[31] A.K. Thapa, K. Saimen, T. Ishihara, Electrochem. Solid-State Lett. 13 (2010) A165–A167.
[32] A.K. Thapa, T. Ishihara, J. Power Sources, doi:10.1016/j.jpowsour.2010.09.112.
[33] M.S. El-Deab, T. Ohsaka, Angew. Chem., Int. Ed. 45 (2006) 5963–5966.
[34] K.Q. Ding, Int. J. Electrochem. Sci. 5 (2010) 668–681.
[35] V. Subramanian, H.W. Zhu, B.Q. Wei, J. Power Sources 159 (2006) 361–364.
[36] F. Hashemzadeh, M.M.K. Motlagh, A. Maghsoudipour, J. Sol–Gel Sci. Technol. 51 (2009) 169–174.
[37] N. Wakabayashi, M. Takeichi, M. Itagaki, H. Uchida, M. Watanabe, J. Electroanal. Chem. 574 (2005) 339–346.
[38] L. Jiang, A. Hsu, D. Chu, R. Chen, J. Electrochem. Soc. 156 (2009) B370–B376.
[39] Y.W. Guigui Wang, D. Chu, R. Chen, D. Xie, J. Membr. Sci. 332 (2009) 63–68.
[40] C.-Y. Chen, S.-C. Wang, Y.-H. Tien, W.-T. Tsai, C.-K. Lin, Thin Solid Films 518 (2009) 1557–1560.
[41] V. Subramanian, H.W. Zhu, R. Vajtai, P.M. Ajayan, B.Q. Wei, J. Phys. Chem. B 109 (2005) 20207–20214.
[42] M.C. Jeong, C.H. Pyun, I.H. Yeo, J. Electrochem. Soc. 140 (1993) 1986–1989.
[43] Y.W. Lee, M. Kim, Y. Kim, S.W. Kang, J.H. Lee, S.W. Han, J. Phys. Chem. C 114 (2010) 7689–7693.
[44] B. Li, J. Prakash, Electrochem. Commun. 11 (2009) 1162–1165.
[45] S.Y. Wang, J.N. Xie, T.R. Zhang, V.K. Varadan, J. Power Sources 186 (2009) 532–538.
[46] K. Gong, D. Su, R.R. Adzic, J. Am. Chem. Soc. 132 (2010) 14364–14366.
[47] W. Sun, A. Hsu, R. Chen, J. Power Sources 196 (2011) 627–635.
[48] F.H.B. Lima, J. Zhang, M.H. Shao, K. Sasaki, M.B. Vukmirovic, E.A. Ticianelli, R.R. Adzic, J. Solid State Electrochem. 12 (2008) 399–407.
[49] K. Jandee, T. Momma, T. Osaka, J. Power Sources (2009) 909–915.